Die Angewandte Makromolekulare Chemie **183** *(1990) 197-220 (3243)*

Dietrich Haarer
Physikalisches Institut und Bayreuther Institut für Makromolekülforschung (BIMF), Universität Bayreuth, Postfach 101251, D-8580 Bayreuth, F.R.G.

PHOTOCONDUCTIVE POLYMERS: STRUCTURE, MECHANISMS AND PROPERTIES

Dietrich Haarer

SUMMARY

Charge carrier transport properties of organic polymers can vary over a wide range. The paper shows that the electron- and hole mobilities of polymers with pendant photoconductive groups (i.e. carbazole) are on the order of 10^{-6} cm^2/Vs. In these materials the flow of electronic charge is maintained by the overlap of the π-orbitals of the pendant molecular groups. The large variation of this short-range interaction, depending on the local configurations encountered in polymer glasses, leads to a large variation of hopping probabilities and, hence, to wide rate-distributions. These distributions are reflected in the slow algebraic decay characteristics of the observed photocurrents. The typical time exponents α ($\alpha \leq 1$) are shown to carry a great deal of physical information, if the dynamical range of the experiments is sufficiently large. The paper also refers to quasi-conjugated polymers (polysilanes) whose dynamic transport parameters are about 10^3 times better (faster) as compared to polymers with pendant groups. These new materials open interesting aspects for the development of new polymeric materials with better transport parameters and, hence, shorter 'switching times'.

Paper presented at the meeting of the CDCh-Fachgruppe "Makromolekulare Chemie" on "Polymers and Light" in Bad Nauheim (W-Germany) May 7-9, 1990.

 CCC 0003-3146/90/$ 03.00

1. INTRODUCTION

One of the few, if not the only electronic application, where polymers are superior or equivalent to amorphous semiconductors is the application as photoconductive media in the field of Xerography, laser-printing or the fabrication of offset-printing masters. In these applications the superb dielectric qualities of polymeric materials are exploited together with a good quantum yield for electron-hole separation and reasonable charge carrier transport properties. The above materials parameters are of rather different nature reflecting the fact that photoconduction phenomena are complex and the 'overall performance' of a material is based on a variety of different processes which may, from a mechanistic viewpoint, have nothing or little in common.

The fact that the critical combination of materials parameters of polymeric photoconductors is surprisingly good is supported by Fig. 1, which shows the overall light sensitivity of various organic and inorganic materials /1/. Polymeric photoconductors are almost as light-sensitive as photographic materials and have a much higher sensitivity than straight forward photo-reactive polymers. This fact is intimately related to a 'gain mechanism' which will be discussed below; however, it reconfirms the fact that photoconduction is a complex phenomenon with diverse elementary processes involved.

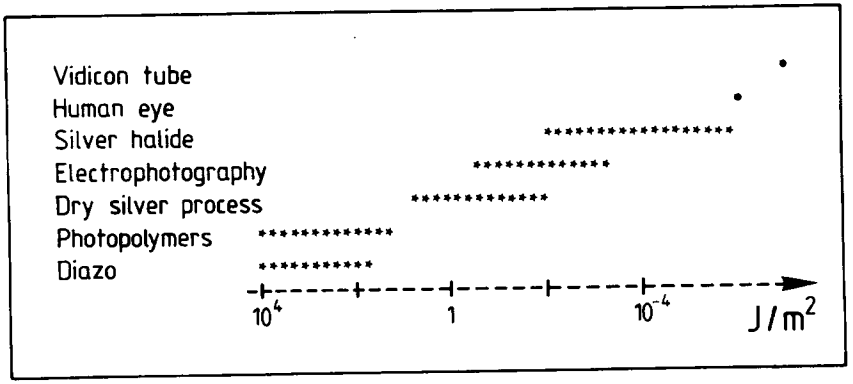

Fig. 1. Light sensitivity of various technically used materials, compared to the sensitivity of the human eye.

Historically the first application of polymeric photoconductors was reported in the field of Xerography which was, until the early seventies, dominated by the use of inorganic photoconductors especially amorphous selenium /2/. In the early /3/ and late /4/ sixties it became evident that organic polymers with pendant electron-donating groups (polyvinyl-carbazole; PVK) form rather efficient photoconductors if doped with electron-acceptors (like trinitrofluorenone; TNF); the latter form charge-transfer complexes with the host polymer.

The formation of an organic CT-complex (charge transfer) has two obvious advantages: First, the lowest electronic absorption of the material is shifted from the near UV-range to the visible range (formation of a CT-band); second, the quantum yield for electron-hole formation which governs the overall sensitivity of the material is higher for polar, more delocalized excited CT-states as compared to excited states which are localized at the molecular units of a polymeric species. The optimization of organic photoconductors (for review see /5/ and references) and their increasing use, as compared to their inorganic counterparts, was favored by the following properties of organic materials:

a) Less toxicity as compared to some inorganic compounds (like selenium).
b) Ease of fabrication of thin polymer films with tailored optical absorption spectra (various CT-complexes and dye sensitization).
c) Good dielectric properties of organic thin films to maintain high electric fields as required by the electro-photographic process.

Fig. 2 shows the main steps involved in the electro-photographic process; it also reflects the variety of properties which have to be optimized in order to optimize the complete process.

Step 1:
A polymer layer (typically 10 μ; on top of an aluminized polyester sheet) is homogeneously charged via corona-charging (voltages on the order of 1.000 V). During this charging procedure the material has to withstand fields which are on the order of 10^6 V/cm over an extended period of time.

Step 2:
Illumination of the photoconductor leading to free electron-hole pairs, with a high quantum yield. In the figure the holes have to traverse the film and the electrons eliminate the positive corona charge at the surface of the photoconductor.

Step 3 and 4:

In these two consecutive steps the electrostatic picture which was created in step 2 is 'developed' with electrostatically charged toner particles and can subsequently be transferred to the paper and 'fixed' by fusing the toner particles to the paper with an IR light source.

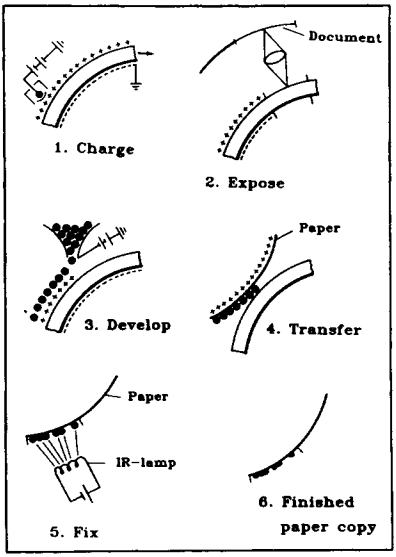

Fig. 2. Principle of the electro-photographic process: 1. corona charging, 2. exposure of photoconductor, 3. development process, i.e. transfer of charge carriers through the photoconductive layer and electrostatic transfer of toner particles, 4. transfer of toner particles to the paper, 5. thermal fusion of toner particles to the paper, 6. finished paper copy.

If the toner particles are fused to the photoconductor (omitting step 4) the photoconductor surface itself can be used as offset printing master /6/.

The description of the complex processes of 'electro-imaging' makes it obvious that in this review only recent developments can be described, showing improvements of the theoretical understanding of some special aspects of photoconductivity in amorphous media and of approaches to new polymeric materials with improved electro-optic properties.

2. BASIC PROCESSES OF THE PRIMARY ELECTRON HOLE SEPARATION

The first step in the sequence of processes leading to photoconduction occurs on a sub-picosecond timescale. It is the light-induced electron-hole

separation which, eventually, leads to free charge carriers which can be utilized to charge or discharge a given polymer surface. The mechanistic details of electron-hole separation are not well understood yet; however, they can be reasonably described by a mesoscopic model, the 'Onsager model' which describes the diffusion of an electron-hole pair (or ion pair) in their mutual Coulomb-field under an external applied electric field. The only adjustable parameter of this model is the 'initial' electron-hole separation radius r_0 at which the thermal diffusion process is 'switched on'.

The Onsager equation, as given by equation 1(a) /7/ cannot be solved analytically.

$$\frac{\partial f}{\partial t} = \frac{kT}{e}\,\mu\,\mathrm{div}\left[\exp\left(\frac{U}{kT}\right)\,\mathrm{grad} f\left(\frac{U}{kT}\right)\right] \qquad (1.a)$$

$$U = -\frac{e^2}{4\pi\varepsilon\varepsilon_0 r} - eEr\cos\theta \qquad (1.b)$$

f is the probability for electron-hole separation and U is the potential, as defined by equ. 1(b), where E is the electric field, r the electron-hole distance and θ the angle between the field lines and the distance vector r.

Numerical solutions of equ. 1 were used in the seventies to treat electron-hole separation in molecular crystals /8,9/. The efforts to apply the same Onsager-equation to polymers were only partially successful since the accessible field range was rather limited /10/. Experiments with an extended field range were carried out for polyvinyl carbazole (PVK) and have been presented recently /11/; these data reconfirmed the notion that the Onsager-theory can be applied successfully to fit the experimental data. Fig. 3 shows numerical calculations of the electron-hole quantum yield over a wide field range with experimental data for PVK. The scatter of the experimental data is due to the difficulty of defining accurate field strengths in an insulator in the presence of residual space charges (especially at low field values). The experimental results, however, corroborate the calculations which predict quantum yields of 10^{-4} to 10^{-5} at low field strengths and values on the order of unity ($\approx$ 0.5) at fields on the order of 10^6 V/cm or higher.

Fig. 3 also reflects in an impressive way that high quantum yields (on the order of unity) require in organic materials extremely high fields. This condition can be realized rather conveniently for applications in the field of photoconduction where external voltages are applied, however, the same

favorable conditions cannot be realized for photovoltaic applications where one has to work with internal field made up by Schottky-barriers (which are problematical in polymeric solids).

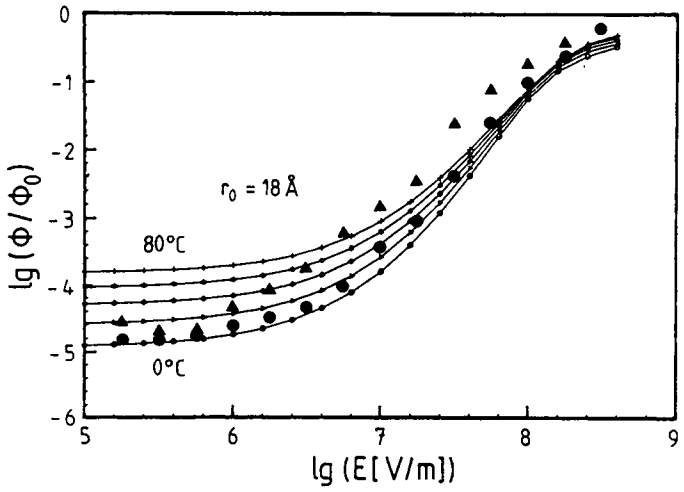

Fig. 3. Onsager ionization probability (see text) as calculated for temperatures between 0° C (lower curve) and 80° C (top curve; increments 20° C). The experimental points for 0° C (circels) and for 80° C (triangles) are superimposed (see text).

In spite of the seemingly pleasant agreement between theory and experiment, there are still open questions as to the 'molecular' interpretation of the results. The r_0 fit-parameter of the Onsager-model for PVK yields 18 Å for the 'initial distance' of the electron hole pair; this value is considerably larger than a typical exitonic radius i.e. the primary radius of an electron-hole excitation. These molecular radii are symbolicly shown in Fig. 4 for a molecular state (carbazole) and for a charge transfer state (CT-state; trinitrofluorenone-carbazole); they are on the order of 3-5 Å (Frenkel states). The microscopic understanding of the processes which play a role in the sequence which starts with excitonic Frenkel states and then yields more loosely bound 'Onsager-states' (20 Å) is not yet at a satisfactory level. The large Onsager-radii which are typical of most organic materials /8,9,10/ also reflect the fact that the 'mesoscopic' if not macroscopic nature of the Onsager-model has only limited applicability for states which have 'molecular dimensions' such as Frenkel excited states. Further understanding of these phenomena will require sub-picosecond techniques which are in the process of being developed (see for instance ref. /12 and 13/ with references).

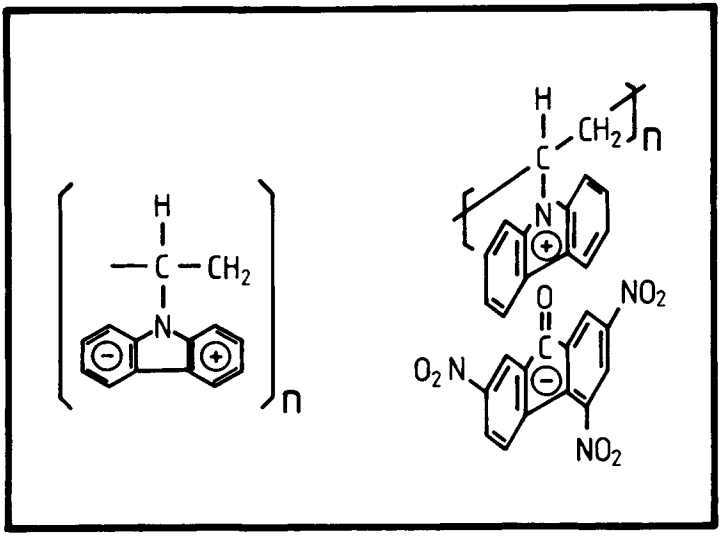

Fig. 4. Schematic répresentation of an excitonic state in PVK (polyvinylcarbazole) and of a CT-exciton in PVK-TNF (trinitrofluorenone).

3. CHARGE CARRIER TRANSPORT

3.1. Technical Relevance of Charge Carrier Transport

One of the key mechanisms of the various applications of organic photoconductors is the separation of electron-hole pairs over macroscopic distances as can be seen in Fig. 2; the final electron-hole separation has to reach distances on the order of 10 μ or larger in order to discharge a polymeric photoconductor through its back electrode. This distance is 10.000 times larger than the typical Onsager dimensions, yet, it is typical for most technical electronic devices.

One main reason why photoconductors are so efficient is the fact that large external electric fields can be applied in the technical process. These fields lead to high carrier efficiencies as described in the previous section; they also provide a good energy balance of the technical process of photoconduction. If we assume that the photon which was used to create an electron-hole pair deposites on the order of 2 eV of energy for each charge carrier (assuming a quantum yield of about 1), then the 'external battery', as provided by the corona charge of Fig. 2, has to provide another 1.000 eV of energy

to transport the free carrier through the organic film (electron or hole, depending on the polarity of the corona).

If we would define a 'gain factor' in such a way that we compare the energy which an external battery provides for the technical process of photo-imaging (1.000 eV) with the genuine photon energy (2 eV) we would formally arrive at a gain factor on the order of 10^3. This high gain factor is one of the reasons, why electro-photography turns out to be such a sensitive application of organic materials. It is, to our knowledge, one of the few technical processes in the field of organic materials with a sizeable gain factor. The above gain process resembles, in a way, some of the gain processes which are used in biological systems, where the chemical energy of an external system (here corona-charging) is used to amplify a primary process which carries the information of the system. In this spirit, the scheme depicted in Fig. 2 can be looked upon as a device which efficiently transfers a 'photon image' into an 'electron image'. The latter can be used for electrostatic printing techniques.

3.2. Experimental Determination of Charge Carrier Transport under Constant Mobility Conditions

The easiest way to visualize charge carrier transport is given in the picture of a TOF-experiment /14,15/ (Fig. 5). Here a short pulse (10 ns in Fig. 5) creates electron-hole pairs in the immediate vicinity of the front electrode (left electrode in Fig. 5). The thickness of the charge generation layer is, for homogeneous materials, defined by the penetration depth of the light. This penetration depth is on the order of 0.5 μ if one uses UV-light and polymers with pendant carbazole groups (like for instance PVK). If the thickness of the sample is on the order of 10 μ, one can consider the initial charge carrier distribution as a quasi two-dimensional sheet.

In the process of the absorption of a light pulse within the surface layer of the sample, charge carriers are formed as electron-hole pairs, according to the mechanisms as described in chapter 2. Depending upon the polarity of the external field one charge carrier species (electrons in Fig. 5) will be discharged right away due to their vicinity to the front electrode. The oppositely charged species, however, has to traverse the bulk of the sample (holes in Fig. 5). This transport over a distance on the order 10 μ or more can be considered as a macroscopic distance. As the charge carriers traverse this distance, they give rise to a 'displacement current' which can be measured in an external electrical circuit. This current is constant, if one assumes a constant mobility of the charge carriers (which is not given for

most polymers; see below) and falls off to zero at a time τ_t at which the charge carriers arrive at the back electrode. Due to a certain spreading of the charge carriers, as caused by diffusion processes, and due to the finite penetration depth of the light, the falloff at τ_t is somewhat smeared out as shown in Fig. 5. Fig. 5 also makes an implicit assumption:

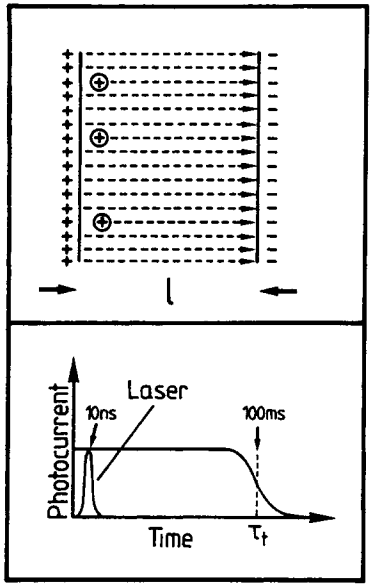

Fig. 5. Symbolic description of TOF-experiment. The laser pulse and the induced photocurrent for nondispersive transport (see text) are given in the lower part of the figure.

It is assumed that the number of charge carriers which form the total charge Q (see equ. 4) is small enough, so that they do not distort the external field considerably. This condition is quantitatively fulfilled if equ. 2 holds.

$$Q \ll C V_B \qquad (2)$$

Here C stands for the capacitance of the sample and V_B is the external voltage across the sample ($V_B = E \cdot l$ according to our definitions as given above).

The time of flight experiment, as shown in Fig. 5, is typically performed with polymer samples as depicted in Fig. 6. Here the front electrode is a semitransparent aluminum layer allowing a top-illumination geometry.

If we assume, for simplicity, a constant mobility μ the charge carriers have a constant drift velocity $v_d = \mu E$ and, thus,

$$\tau_t = \frac{l}{E\mu} = \frac{l^2}{V_B\mu} \qquad (3)$$

the area under the current-time diagram yields the total number of charge carriers Q involved in this transport process due to the relation

$$Q = \int_o^\infty I \, dt \qquad (4)$$

where I is the current in the external circuit.

For the conditions of a constant (i.e. time independent) mobility μ the characterization of the electron or hole transport can be carried out using the above TOF-experiment and its rather straight forward interpretation.

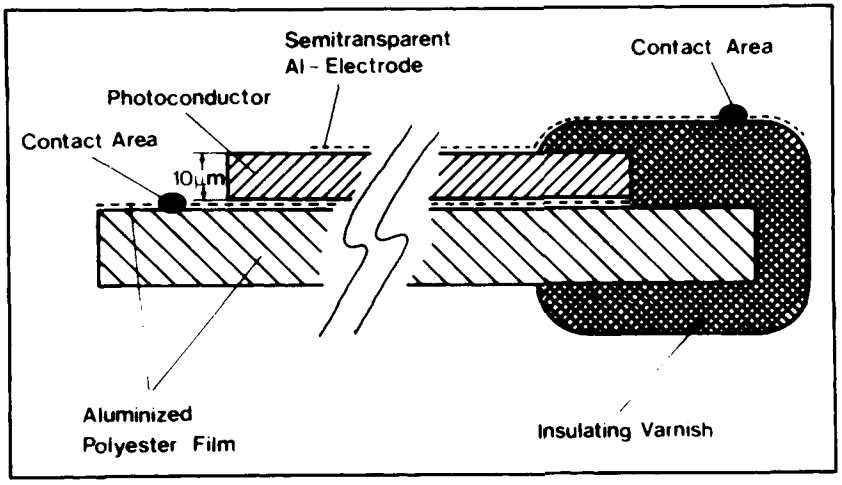

Fig. 6. Sample cross section. The photoconductor layer is on top of an aluminized polyester film. The insulation varnish prevents electrical breakdown at the edge of the sample. The top electrode is a semi-transparent, evaporated aluminium film.

Fig. 7 shows two TOF-curves for an organic CT-crystal at two different applied fields. In both cases, the transit times τ_t are well defined (in the millisecond regime for crystals of thickness 1 mm) and allow the determination of a mobility μ (see for instance /16 and 17/). The exponential current decay which is superimposed on the experimental TOF-curves distinguishes the experimental curves from the idealized TOF-curves (Fig. 5); it is due to charge carrier trapping reducing the total number of freely mobile charge carriers. This trapping phenomenon, however, does not interfere with an accurate determination of the mobility values of crystalline materials.

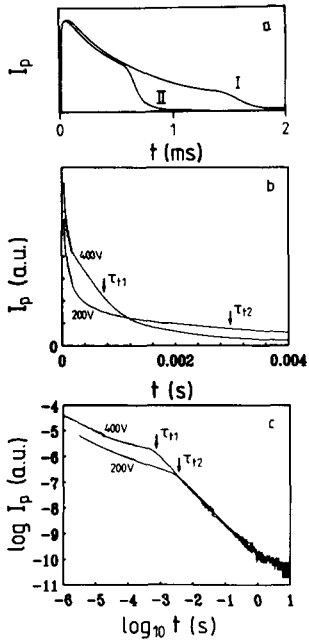

Fig. 7. a) Photocurrent in the molecular CT-crystal anthracene-PMDA for two applied voltages (I = 1000 V; II = 2500 V; the sample thickness was 1.2 mm. b) Photocurrent in the polymer siloxane at an applied voltage of 200 V and 400 V (thickness 10 μ). c) Same data as above but plotted on a log-log plot.

For amorphous materials the situation is much more involved. Here a straight forward TOF-experiment, as carried out with a carbazole substituted sixolane polymer (see insert in Fig.17) is given in Fig. 7b. On a linear I-t-plot there is no visible break in the photocurrent curve and, thus, the experiment does not allow a straight forward determination of the transport parameter μ. Plotting the same data on a log-I versus log-t plot, however, shows a marked change of slopes of the photocurrent at times τ_{t1} and τ_{t2} (Fig. 7c). Now an 'effective mobility' can be defined by using equ. 3. This definition, however, was only possible by interpreting the experiments with a theory of Scher and Montroll, as described in the next section /18,19/.

3.3. Dispersive Transport; Time Dependent Mobilities

In materials with periodic structures one can visualize the transport of a charge carrier in an external field as a diffusion process with a superimposed drift term in field direction. The only part of the carrier movement which affects the external current is the mono-directional drift part (in field

direction). If we describe this drift propagation in a one-dimensional picture and assume a constant 'hopping probability' in field direction, one can define a function $\hat{\Psi}(t)$ which is the probability that the charge carrier performs a field-induced jump in the time interval between t and $t + \Delta t$. In the simplest case the $\hat{\Psi}(t)$ function falls off monoexponentially as

$$\hat{\Psi}(t) = W \exp\{-Wt\} \tag{5}$$

Here W is a given probability value which will be a function of the lattice geometry, the molecular wave functions and the applied electric field. The situation in an ordered material may be well described by a $\hat{\Psi}(t)$ as given above; in a disordered material, however, charge carriers at different 'sites' i.e. different local environments would be characterized by different $\hat{\Psi}(t)$ functions. In the CTRW-approach, as proposed by Scher and Montroll /18,19/, a charge carrier ensemble can be characterzied by a broad distribution of hopping probabilities and, thus, the $\hat{\Psi}(t)$-function can be written as

$$\Psi(t) = \int_{\varepsilon} g(\varepsilon) W(\varepsilon) \exp\{-W(\varepsilon)t\} \tag{6}$$

where g (ε) is the distribution function, characterizing the contributions of the various decay terms $\hat{\Psi}(t)$. The parameter ε is an energy parameter, indicating that there is a correlation between the hopping probability W and the energy ε of a given state (see below). It was the merit of Scher and Montroll and Scher and Lax /18,19/ to realize that the $\Psi(t)$-function, as given above, falls off with an algebraic power law in case of a wide distribution of the $W(\varepsilon)$ parameters.

$$\Psi(t)|_{t\to\infty} \sim t^{-(1+\alpha)} \tag{7}$$

In the above equation the main physical information about the dynamical properties of the system is contained in the α-parameter.

To fill the α-parameter with some content, the general formalism of the Scher-Montroll-theory can be discussed within the framework of a theory based on energy level distributions as has been shown by Schmidlin and Noolandi /20,21/. Instead of assuming a one-dimensional hopping process with a general $\Psi(t)$-distribution (Fig. 8a) one can visualize the charge carriers as propagating in a narrow conduction band (in field direction as symbolized by the slope of the conduction band in Fig. 8b). The mobility of the carriers is governed by trapping and detrapping processes into an exponential distribution of trapping states below the conduction band. This microscopic model makes following assumptions:

First, the carriers arriving at a trap get trapped instantaneously with probability one.

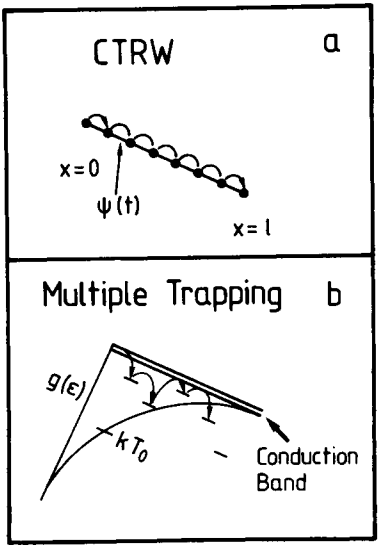

Fig. 8. a) One dimensional model for CTRW (continuous time random walk) $\Psi(t)$ is the probability that the charge carrier jumps in field direction in the time interval between t and t + Δt. b) Multiple trapping model. The charge carrier is trapped and can be released via Boltzmann-activation. The trap distribution g(ε) is exponential with a falloff constant in energy space of kT_0.

Second, the release of the trapped carriers is governed by a Boltzmann-activation process according to the following relation

$$W(\varepsilon) = W_o \exp\{-\varepsilon/kT\} \qquad (8)$$

where W_0 is an attempt-to-jump probability. This simple picture relates the rates W with an energy scale ε in the most simple fashion. It also assumes quite often, for the sake of simplicity, an exponential trap distribution falling off by the factor 1/e in an energy interval kT_0 as shown in Fig. 8b.

With the above assumptions equ. 6 can be rewritten in an explicit form

$$\Psi(t) \sim \sum_{\varepsilon} \exp\{-\varepsilon/kT_o\} \exp\{-\varepsilon/kT\} \exp\{-\exp(-\varepsilon/kT)W_o t\} \qquad (9)$$

Here we have, for simplicity, omitted normalization factors. Note, that the energy parameter ε appears in both, the density of state function g (ε) as well as the $\Psi(t)$-function. In the latter it appears as exponential in the

exponent which means that the assumption of Boltzmann-activation leads to an extremely strong energy dependence of the dynamic transport parameters.

In recent years the mathematical description of dispersive dynamic processes i.e. of processes which are characterized by wide rate distribution have received a great deal of attention. In this context Shlesinger /22/ has given an expression for the $\Psi(t)$-function which is valid for long times and which casts the dynamical picture into 'time fractals' with

$$\Psi(t) = \sum_{n} a^n b^n \exp\{-b^n t\} \qquad (10)$$

Shlesinger has also shown that the time exponent α can, for long times, be written as

$$\alpha = ln \frac{a}{b} = ln \frac{a^n}{b^n} \qquad (11)$$

With this definition of α we can, by comparison of equ. 6, 9 and 11 write α in a form which contains only simple energetic model parameters

$$\alpha = \frac{ln\ g(\varepsilon)}{ln\ W(\varepsilon)} = \frac{T}{T_0} \qquad (12)$$

With the above mathematical derivations we can summarize that the dispersive kinetics of the CTRW-theory can be cast into a simple form if one assumes 'energetic disorder' i.e. disorder whose origin is linked to the energy position of the involved trapping-states. In such a picture the α-value is given by the ratio of the absolute temperature T and the distribution width T_0 (in units of kT) of a set of exponential traps, controlling the transport through Boltzmann-activation.

In this context it may be interesting to project the Shlesinger model onto a model with hierarchical energy barriers /23/. Taking a hierarchical set of barriers, as shown in Fig. 9, we can ask for the probability W_{ij} for a Boltzmann-activated particle to get from point j to point i. Since the total barrier ΔE_{ij} is made up by n elementary barriers (Fig. 9 is drawn for n = 3) we can formally write W_{ij} as b^n as it is appearing in the 'time fractal'-like expression of Shlesinger as given in equ. 10.

$$Wij = \exp\{-\Delta E_{ij}/kT\} = \exp\{-n\Delta/kT\} = b^n \text{ with } b = \exp\{-\Delta/kT\} \qquad (13)$$

With the above description the set of hierarchical barriers reproduces, if we look at the number-density of barriers, an exponential distribution, as assumed for the simple model.

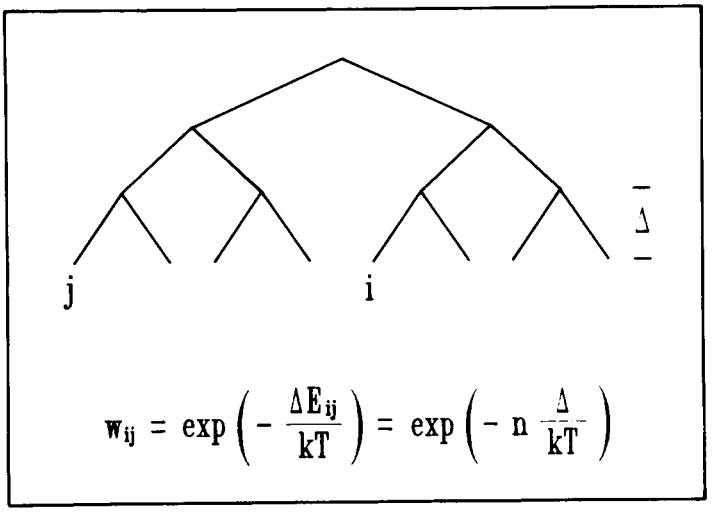

Fig. 9. Hierarchical scheme of energy barriers. The charge carrier can either be activated over a single barrier of height Δ or it can be activated over n barriers. The probability for having to overcome higher barriers falls off exponentially (see text).

3.4. Comparison with Experiment

So far we have used the simplest model description of dispersive transport and have interpreted the algebraic time exponent α of the long-time photocurrents in terms of the model parameters T and T_0. Following this simple description we expect macroscopic photocurrents which can, in a double logarithmic plot, be characterized by two straight lines, whose slope adds up to two and shows a break at the transit time τ_t as depicted in Fig. 10.

If we take the carbazole-substituted siloxanes as examples for materials with dispersive photocurrents /24,25,26/ we see in Fig. 11 that the straight forward dispersive model holds quite well and yields an α-value of about 0.6. α-values which are different from $\alpha = 1$ lead to rather complex phenomena.

1. The effective mobility decreases as a function of time. This phenomenon is common for many disordered systems; it has to do with the fact that the ensemble of charge carriers which is originally produced in a band-state falls, with its center of gravity, deeper and deeper into the exponential funnel of traps. Fig. 12 shows the lowering of energy ε (in units of kT)

as a function of hopping events (parameter) for a one-dimensional calculation /27/.

The calculation also shows, that the maximum of the carrier distribution moves lower in energy on a logarithmic time scale. Such logarithmic time-dependencies are rather common for disordered media.

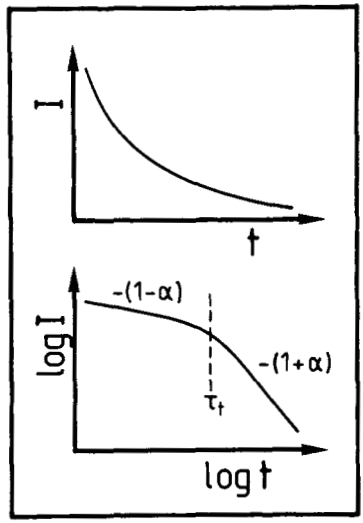

Fig. 10. Linear and logarithmic plot of the photocurrent in a dispersive system. In the logarithmic plot the transit time τ_t is clearly discernible.

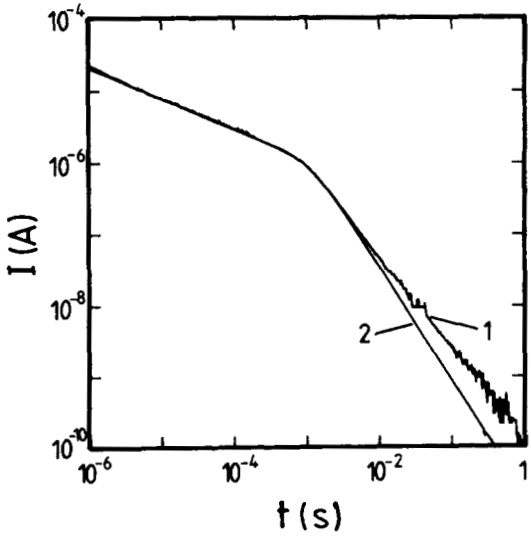

Fig. 11. Transient photocurrent (1) in polysiloxane and theoretical curve (2), calculated from an algebraic $\Psi(t)$ with $\alpha = 0.58$ (double logarithmic plot).

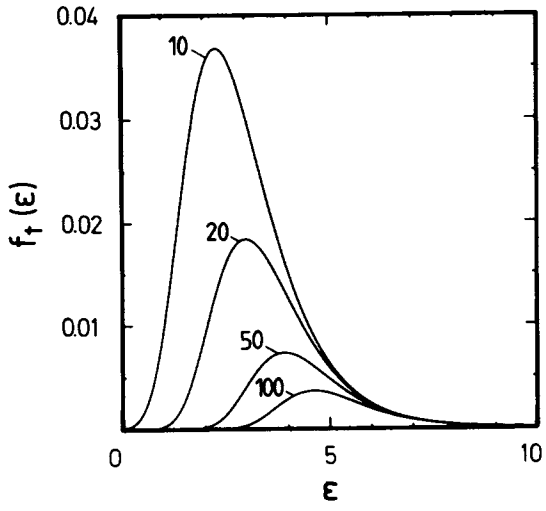

Fig. 12. Weight function $f_t(\varepsilon)$ for the trap population as a function of energy ε and time (the time-parameter labels the various curves /27/; see text).

2. In dispersive materials the characteristic transport times do not scale in a linear fashion with the sample thickness l or with the electric field E. It can be shown that the following relations hold /26/.

$$\tau_t = l^{1/\alpha} \tag{14a}$$

$$\tau_t \sim E^{-1/\alpha} \tag{14b}$$

Fig. 13 shows the field - and thickness dependence of the transit time τ_t for the carbazole substituted siloxane polymer. The figure shows that with an α-value on the order of 0.5 (as given for siloxane) the transit time varies roughly with the square of the sample thickness; with an α-value of 0.25 it would vary with the fourth power of the thickness. These interesting scaling properties have lately attracted considerable experimental and theoretical attention.

So far only the most simple model assumptions, like for instance exponential trap distributions, have been made. For some systems these assumptions are satisfied reasonably well. For other systems, like for instance PVK, those assumptions are less valid and yield time dependent α-values which reflect complex equilibration processes in disordered media.

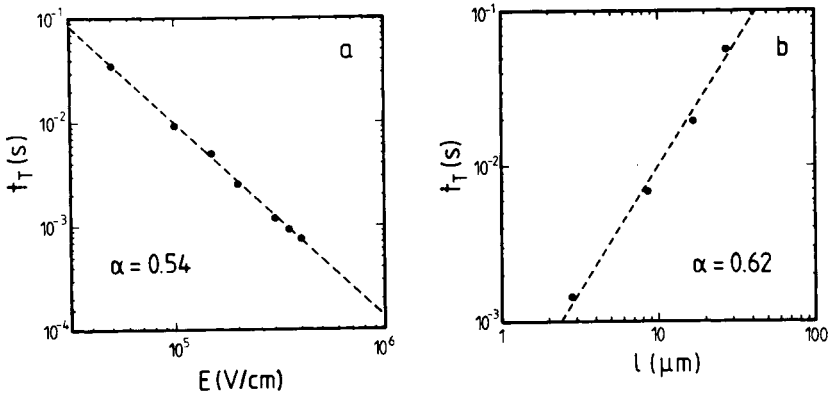

Fig. 13. a) Dependence of the effective transit time τ_t on the electric field strength (see text). b) Dependence of the effective transit time τ_t on the sample thickness l /26/.

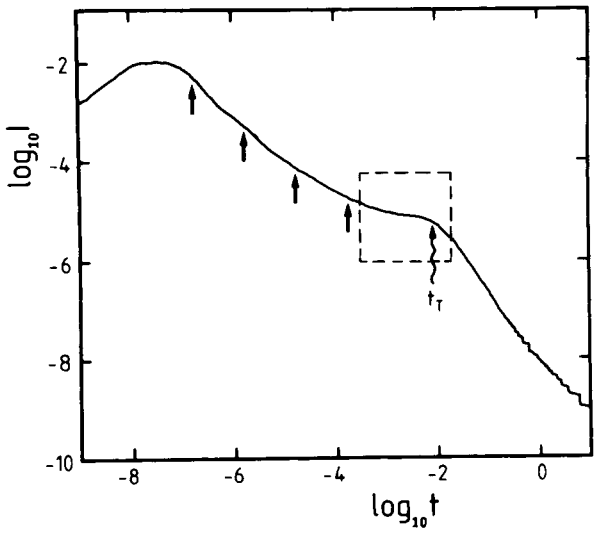

Fig. 14. Photocurrents in PVK over a time interval of 9 decades. The slope of the log-log plot changes from 1 to 0 and, thus, α changes over its full range of α = 0 to α = 1 (see text). The dotted square covers two decades in time and intensity (see text).

Fig. 14 shows the photocurrent for PVK measured over about nine decades in time. Here we see clearly that the slope and, thus, the α-value changes over its whole range of definition from $\alpha = 0$ (slope 1) to $\alpha = 1$ (slope 0). The arrows in the figure indicate the onset of different digitizer systems to yield the large dynamic range of the experiment. The dotted square shows an interval of two time-decades. Within such small time domains a constant α-value which does not reflect the dynamics of the system can be assumed but often has not physical relevance.

For a more extensive discussion of the complex aspects of non-equilibrated amorphous systems we refer to further literature /25,28,29/.

4. NEW MATERIALS; OUTLOOK

There are certain advantages of organic polymeric photoconductors which have been spelled out in the introduction of this paper, however, these materials also have disadvantages as compared to inorganic photoconductive materials like amorphous silicon or selenium: The main disadvantage is the low mobility of organic materials which is several orders of magnitude lower as compared to the mobilities of amorphous silicon or organic crystalline materials (see Fig. 15).

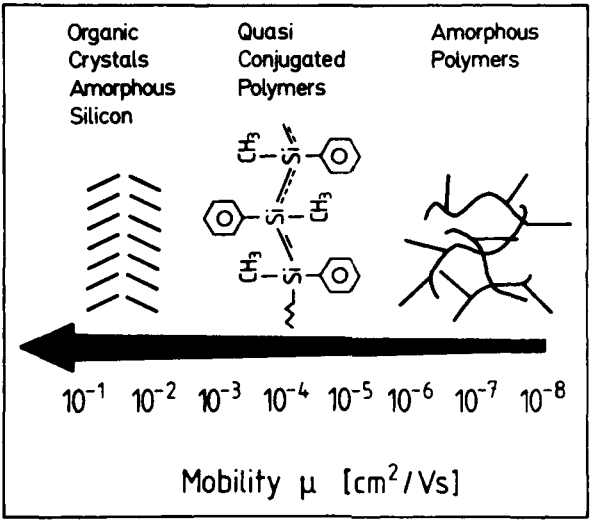

Fig. 15. Mobility ranges of various materials (see text)

Fig. 15 shows that μ-values for amorphous polymers are on the order of 10^{-6} cm^2/Vs i.e. more than six orders of magnitude lower than mobilities of typical amorphous semiconductors. This feature which is mainly due to the dispersive nature of the charge carrier transport, as described above, can be a serious drawback for fast electronic applications. It can, however, be tolerated for most printing- and copying techniques which are basically parallel processing techniques (all picture elements are processed simultaneously). Nevertheless it would be desirable to achieve higher mobilities with organic polymers maintaining other properties and, especially, the materials-variability.

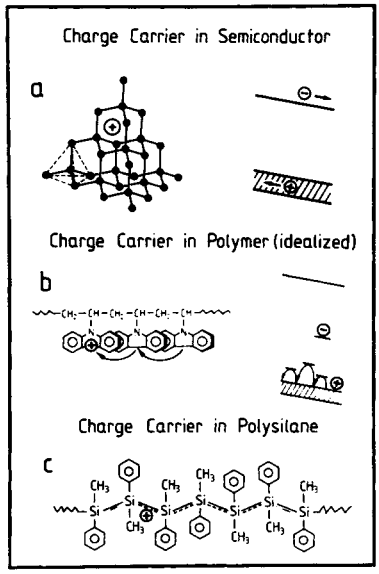

Fig. 16. Schematic representation of a charge carrier in a semiconductor (a; band state), in a polymer (b; hopping conduction) and in a quasi-one-dimensional polymer (c; quasi-conjugation).

A possible way for achieving higher mobilities is shown in Fig. 16 in a schematic fashion. In a crystalline semiconductor one can mostly assume a band-like motion and, thus, trapping phenomena may be of lesser importance or mainly dominate the very short time regime (Fig. 16a). In polymeric materials the charge carrier delocalization is mainly due to the overlap of molecular π-orbitals. These orbitals decay exponentially with the intermolecular distance and, thus, a spatial disorder of the polymeric chains leeds to rather large variations of the hopping time distributions. Therefore a hopping model with traps, as show in Fig. 16b, often describes the main feature of the carrier transport. It is important to note that these traps can, in principle, be either interpreted as 'extrinsic traps' (for instance impurities) or as structural defects (intrinsic traps). For amorphous mate-

rials these intrinsic traps play a major role and, hence, chemical purity reflects only one part of the transport properties of the materials involved. In recent years it has become more and more obvious that structural and configurational defects may play an even more important role. These defects are, to a major extent, not related to chemical purity, but to the preparation techniques of the polymer films (solvents used, evaporation rates, annealing temperatures etc.).

Recently new data non quasi-conjugated and one-dimensional polymers have become available /30,31/ which show rather high mobilities for polysilanes (Figs. 15, 16). For these materials an approach to band-like motion may be feasible.

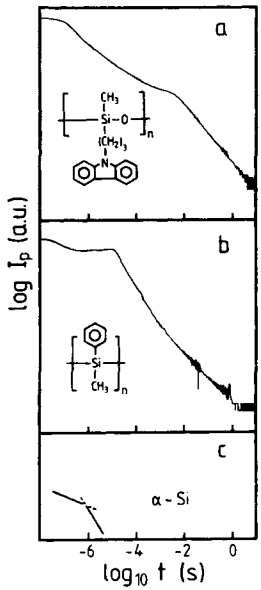

Fig. 17. Photocurrent of various amorphous materials in a log-log plot. a) Siloxane polymers with pendant carbazole groups (see insert). b) Polysilane polymers, see text). c) Amorphous silicon.

Fig. 17 shows our own data on polysilanes /32/ compared to data on siloxanes (dispersive system) and amorphous silicon /33,34/. The experimental parameters such as sample thickness, electric field etc. are comparable for the various materials shown in Fig. 17 and, thus, one gets transit times on the 10 ms scale for polysiloxanes, on the 10 μs scale for polysilanes and on the 1 μs scale for amorphous silicon. Also polysilanes seem to be less dispersive than other polymer systems /30,31,32/ and may thus be looked upon as a step towards organic 'semiconductor-like' materials. In this context one may also think of materials like undoped $(CH)_x$ and other undoped conjuga-

ted polymers. Here higher mobilities may, in principle, be given; yet, chemical stability and dielectric properties may be much less desirable than in 'slower polymers'. Taking these considerations into account, the future development will be given by the optimal tradeoff between chemical, dielectric and photoelectric properties.

ACKNOWLEDGEMENT

I would like to thank A. Blumen and H. Schnörer for many contributions to the understanding of dispersive transport phenomena. I also would like to thank E. Müller-Horsche, H. Kaul, H. Domes and R. Fischer for experimental data and P. Strohriegl and W. Joy for the synthesis and preparation of various polymeric materials. The work was supported by the Deutsche Forschungsgemeinschaft, the Bundesministerium für Forschung und Technologie and the Fonds der Chemischen Industrie. We also thank the BASF Corporation (Dr. Jäckel and Dr. Leyrer) for support.

REFERENCES

1. Methods and Materials in Microelectronic Technology, ed. by J. Bargon, (Plenum Press 1984), pp. 181 ff.
2. C.F. Carlson, US Pat. 2 297 691 (1942)
3. H. Hoegl, O. Sus, and W. Neugebauer, US Pat. 3 037 861 (1962) Hoechst AG
4. D.M. Shattuck and U. Vahtra, US Pat. 3 484 237 (1969) IBM
5. D.M. Burland and L.B. Schein, Physics Today (1986), p. 1
6. Patent: K.-W. Klüpfel, M. Tomanck and F. Endermann, DE-B-11 45 184 (1963)
7. L. Onsager, Phys.Rev. 54, 554 (1938)
8. R.H. Batt, C.L. Braun, and J.F. Hornig, Appl.Opt.Suppl. 3, 20 (1969)
9. R.R. Chance and C.L. Braun, J.Chem.Phys. 64, 3573 (1976)
10. P.J. Melz, J.Chem.Phys. 57, 1694 (1972)
11. H. Kaul and D. Haarer, Ber.Bunsenges. Phys.Chem. 91, 845 (1987)
12. S.D. Phillips and A.J. Heeger, Phys.Rev. B38, 6211 (1988), H. Bleier, S. Roth, J.Q. Shen and D. Schäfer-Siebert ibid. p. 6031
13. J. Kuhl and M. Lambsdorff, Phys.Blätt. 46, 199 (1990)
14. O.H. Le Blanc, J.Chem.Phys. 33, 626 (1960)
15. K.G. Kepler, Phys.Rev. 199, 1226 (1960)
16. D. Haarer and M. Philpott, in: Spectroscopy and Excitation Dynamics of Condensed Molecular Systems, ed. by V.M. Agranovich and R.M. Hochstrasser, Vo. 4, (North Holland 1983), pp. 27 ff
17. D. Massa and N. Karl, Mol.Cryst.Liq.Cryst. 95, 93 (1989)
18. H. Scher and E.W. Montroll, Phys.Rev. B12, 2455 (1975)
19. H. Scher and M. Lax, Phys.Rev. B7, 4491, 4502 (1973)
20. F.W. Schmidlin, Phys.Rev. B16, 2362 (1977)
21. J. Noolandi, Phys.Rev. B16, 4466 (1977)
22. M.F. Shlesinger, J.Stat.Phys. 36, 639 (1984)
23. A. Blumen, J. Klafter, and G. Zumofen in: Optical Spectroscopy of Glasses, ed. by I. Zschokke (Reidel, Dordrecht, Holland (1986), p. 199
24. H. Domes, R. Fischer, D. Haarer, and P. Strohriegl, Makromol.Chem. 190, 165 (1989)
25. H. Schnörer, D. Haarer, and A. Blumen, Phys.Rev. B38, 8097 (1988)
26. H. Schnörer, H. Domes, A. Blumen and D. Haarer, Phil.Mag.Lett. 58, 101 (1988)
27. H. Schnörer, Diplomarbeit, Bayreuth 1987
28. E. Müller-Horsche, D. Haarer, and H. Scher, Phys.Rev. B35, 1273 (1987)

29. Festkörperprobleme, Vol. 30, pp. 157-182 (1990) Vieweg Verlag
30. R.G. Kepler, J.M. Zeigler, L.A. Harrah, and S.R. Kurtz, Phys.Rev. B35, 218 (1987)
31. M. Abkowitz and M. Stolka, Polym. for Adv. Technologies 1, 225 (1990)
32. H. Kaul and D. Haarer, unpublished results
33. P.B. Kirby and W. Paul, Phys.Rev. B25, 5373 (1982)
34. J.H. Yoon and C. Lee, J.Non-Cryst. Solids 105, 258 (1988)